EUROPEAN LABORATORY FOR PARTICLE PHYSICS

CERN - LHC DIVISION

LHC-VAC/OBM

Vacuum Technical Note 99-14
October 1999

Estimates of Photon Induced Gas Densities in the Long Straight Sections of IR1 and IR5 for v6.0 of the LHC

O.B. Malyshev and I.R.Collins

1 Introduction

A long straight sections (LSS) of the LHC is defined as a section between two adjacent dispersion suppressors (ending at Q7), encompassing an interaction point (IP). In this Note we concentrate on the matching sections of LSS1 and LSS5 including Q7 to D2. D1, the inner triplet and the experimental vacuum chambers will be studied in a future Notes. Since the optics layouts of LSS1 and LSS5 are identical and symmetric about their IP, apart from the slope of the machine, it is convenient to consider only one side. A schematic of the optics version 6.0 (v6.0) of the left-hand-side (lhs) of LSS1 is shown in Figure 1.

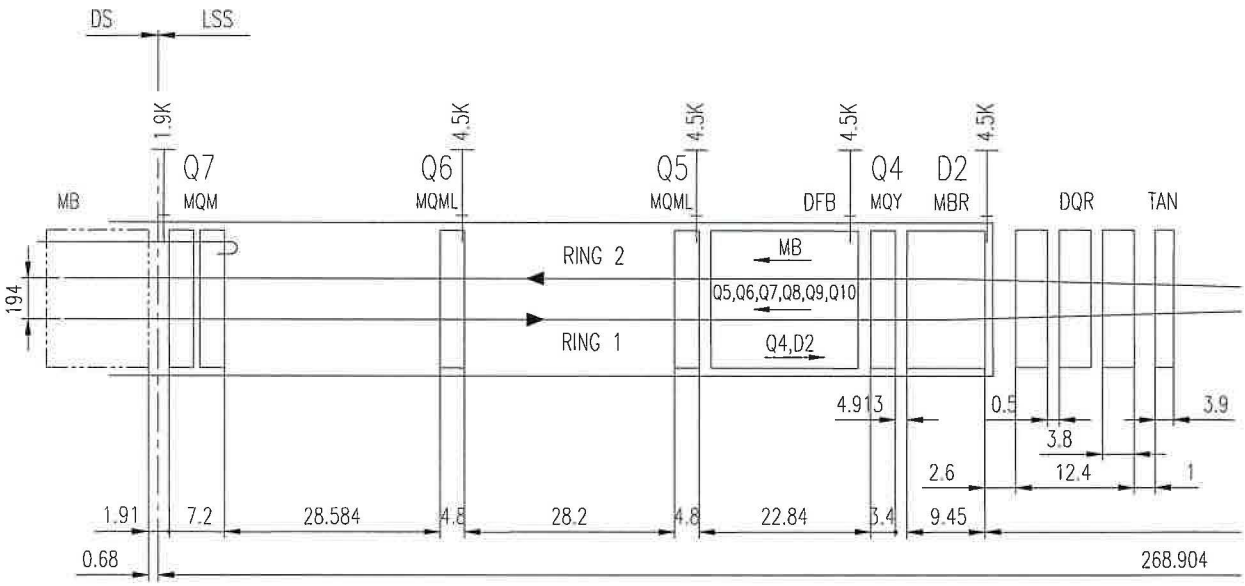

Figure 1. Schematic of the LSS lhs in IR1 and IR5.

The operating temperatures, apertures, total magnetic lengths and presence of beam screens for optics v6.0 are shown in Table 1. It is assumed that all the vacuum chambers between elements at cryogenic temperatures, *i.e.* in connecting cryostats, are at either 4.5 K or 1.9 K and contain a beam screen. LSS1 or LSS5 are ideal cases to estimate gas densities since there exist elements at a number of different operating temperatures and apertures. A previous study of the SR in the LSS in IR1 and IR5 was made for optics v1.0 and is therefore no longer applicable [1]. In this study we focus our attention on the gas desorption produced by the synchrotron radiation

(SR) in the region of the arc to D2 inclusive. A study of ion induced gas desorption, ultimately determining vacuum stability, will be made in a future Note. SR in ring 1 of Figure 1, produced in the arc and dispersion suppressor, enters the LSS and is diluted in intensity as a function of distance from the arc. SR is also produced downstream from the quadrupole magnets when the beam is off-axis and downstream of the separation magnets D1 and D2.

Table 1. Operating temperatures, apertures, total magnetic lengths and presence of beam screens in optics v6.0 of LSS in IR1 and IR5.

Element	Name	Temperature (K)	Aperture (mm)	Length (m)	Beam screen
Inner Triplet	Q1	1.9	∅ 46	30.6	No
	Q2a and Q2b	1.9	∅ 60		No
	Q3	1.9	∅ 60		No
Cryogenic Feedbox	DFB	4.5	∅ 76	5.23	No
Separation Magnets	D1	300	55x130	23.9	No
	D2	4.5	∅ 73	2.438	No
Matching Section	Q4	4.5	∅ 50	3.4	No
	Q5	4.5	∅ 50	4.8	No
	Q6	4.5	∅ 50	4.8	No
	Q7	1.9	Beam screen (∅ 45, H=36)	7.2	Yes

The purpose of this Note is to:

1) estimate the gas densities (H2 and CO) for optics v6.0.

2) estimate the gas densities (H2 and CO) for various operating conditions, namely 1.9 K and 4.5 K, with and without beam screens.

3) determine the necessity of beam screens and/or beam pipe temperature.

4) provide an estimation of the gas densities in the LSS1 and LSS5 that can be used in future studies to determine the vacuum stability due to ion induced desorption.

2 Considerations

Studies of molecular gas desorption using SR on vacuum chambers held at cryogenic temperatures began in 1991. The results of these studies are used to predict the residual gas density inside the LHC vacuum chamber with walls at cryogenic (liquid helium) temperatures irradiated by SR. The gas density inside such a vacuum chamber, *i.e.* with cryosorbing walls, consists of three parts: (1) primary photodesorption of gas, (2) photodesorption of molecules cryosorbed on vacuum chamber walls (secondary desorption) and (3) thermal desorption (equilibrium gas density). A simple model, whose input parameters are determined experimentally, has been formulated to describe the behaviour of such a vacuum system when subject to SR. This model is described in detail in section 3. The proposed beam screen in the arc of the LHC, held at between 5 and 20K inside the cold bore of the superconducting magnet, has two important advantages. It reduces the heat load at 1.9K by intercepting the SR power and carrying the beam induced image current and it provides 'shadow' for the weakly bound cryosorbed (physisorbed) molecules from the SR. This concept is extended and adapted to the LSS.

3 A model of the photodesorption process in a vacuum chamber with cryosorbing walls

The equations of gas dynamic balance inside a vacuum chamber exposed to SR can be written as [2,3]:

$$V\frac{dn}{dt} = \eta\dot{\Gamma} + \eta'(s)\dot{\Gamma} - \alpha S(n - n_e(s,T)) - Cn + A_c D\frac{d^2 n}{dz^2}; \tag{1}$$

$$A\frac{ds}{dt} = \alpha S n - n_e(s,T)) - \eta'(s)\dot{\Gamma}; \tag{2}$$

where n *[molecules/cm^3]* is the volume gas density;

s *[molecules/cm^2]* is the surface density of cryosorbed gas;

V *[cm^3]* is the vacuum chamber volume;

$A\ [cm^2]$ is the vacuum chamber wall area;

$\dot{\Gamma}$ *[photon/sec]* is the photon intensity;

η *[molecules/photon]* is the primary photodesorption yield;

η' *[molecules/photon]* is photodesorption yield of cryosorbed molecules (so-called secondary photodesorption yield);

α is the sticking coeffecient;

$S = A\bar{v}/4$ is the ideal wall pumping speed, $\bar{v}$ is the mean molecular speed;

$C = \rho k_t S$ is the distributed pumping speed of holes, ρ is the Clausing factor for the holes;

$n_e\ [molecules/cm^3]$ is the thermal equilibrium gas density;

A_c is the vacuum chamber cross section and

D is the Knudsen diffusion coefficient.

Hence, in the common case, the gas density in the presence of SR inside the cryogenic vacuum chamber is a function of several unknown parameters that have to be determined experimentally:

$$n = n(\eta, \eta', \alpha, n_e, \bar{v}, s). \tag{3}$$

In the quasi-static condition with $V\frac{dn}{dt} \approx 0$ and $A_w\frac{ds}{dt} \approx 0$ the gas density is described by a simple second order differential equation for $n(z)$:

$$\eta\dot{\Gamma} + \eta'(s)\dot{\Gamma} - \alpha S(n - n_e(s,T)) - Cn + A_c D\frac{d^2 n}{dz^2} = 0. \tag{4}$$

Its solution is of the form

$$n(z) = n_{\inf} + C_1 e^{a\cdot z} + C_2 e^{-a\cdot z}, \tag{5}$$

where n_{inf} is the solution for infinity long tube and $a = \sqrt{\frac{\alpha S + C}{A_c D}}$, the constants C_1 and C_2 are dependent on the conditions at the ends.

In the following sections we consider the solutions for various vacuum chambers: long and short, with and without a beam screen, and their combinations.

3.1 The solution for the infinity long vacuum chamber

In this case there is no axial diffusion it is possible to set $A_c D\frac{d^2 n}{dz^2} \approx 0$.

3.1.1 A vacuum chamber without a beam screen: $C = 0$

The gas density inside a simple vacuum tube is given by:

$$n = \frac{\eta\dot{\Gamma}}{\alpha S} + \frac{\eta'\dot{\Gamma}}{\alpha S} + n_e \tag{6}$$

The second and third terms of (6) depend on the surface density s of cryosorbed molecules:

$$s(t) = s_0 + \frac{1}{A_w}\int_{t=0}^{t} \eta\dot{\Gamma}\cdot dt\,. \tag{7}$$

3.1.2 A vacuum chamber with a beam screen: $C > 0$

The quasi-static solution with $V\frac{dn}{dt} \approx 0$ and $A\frac{ds}{dt} \neq 0$:

The expression for the density inside a vacuum chamber with a beam screen, for the common case is:

$$n = \frac{\eta\dot{\Gamma} + \eta'\dot{\Gamma} + \alpha S n_e}{\alpha S + C}\,. \tag{8}$$

The growth of the surface density, s, on a surface of a beam screen is limited by the distributed pumping, C, and is defined by:

$$s(t) = s_0 + \frac{1}{A}\int_{t=0}^{t}\left(\eta\dot{\Gamma} - Cn(t)\right)dt\,. \tag{9}$$

The expression for the gas density inside the beam screen can also be written in another form:

$$n = \frac{\eta\dot{\Gamma}}{C} - \frac{A}{C}\cdot\frac{ds}{dt}\,. \tag{10}$$

In the equilibrium state when the condition $A\dfrac{ds}{dt} = 0$ is satisfied the gas density depends only on η:

$$n = \frac{\eta\dot{\Gamma}}{C}\,. \tag{11}$$

3.2 The solution for a finite length vacuum chamber without a beam screen between two vacuum chambers with a beam screen

Consider a vacuum chamber centered at $z = 0$, of length L. The conditions at the ends are:

$$n(\pm L/2)=n_{bs}(\pm L/2), \qquad dn(\pm L/2)/dz=dn_{bs}(\pm L/2)/dz.$$

In this case $n(z)$ is given by:

$$n(z) = n_t + \frac{b(n_{bs} - n_t)\cosh(az)\sinh\left(\dfrac{bL}{2}\right)}{b\sinh\left(\dfrac{bL}{2}\right)\cosh\left(\dfrac{aL}{2}\right) + a\sinh\left(\dfrac{aL}{2}\right)\cosh\left(\dfrac{bL}{2}\right)}, \tag{12}$$

here n_t is the solution for an infinity long vacuum chamber without a beam screen and n_{bs} is the solution for an infinity long vacuum chamber with a beam screen;

$$a = \sqrt{\frac{\alpha_t S}{A_c D}} \text{ and } b = \sqrt{\frac{\alpha_{bs} S + C}{A_c D}}\,,$$

where α_t and α_{bs} are the sticking probabilities of a simple tube and a beam screen respectively.

3.3 The solution for a finite length vacuum chamber in an equilibrium state

In the equilibrium state when conditions $V\frac{dn}{dt} \approx 0$ and $A\frac{ds}{dt} \approx 0$ are satisfied and $C = 0$ we can obtain from equation (2) for the dynamic gas balance that

$$\alpha S(n - n_e(s,T)) - \eta'(s)\dot{\Gamma} = 0. \tag{13}$$

Then the first equation of the dynamic gas balance becomes a very simple differential equation:

$$\frac{d^2 n}{dz^2} = -\frac{\eta\dot{\Gamma}}{A_c D}. \tag{14}$$

The solution is:

$$n(z) = -\frac{\eta\dot{\Gamma}}{2A_c D} z^2 + C_1 z + C_2, \tag{15}$$

the constants C_1 and C_2 are depend on the conditions at the ends. Consider a vacuum chamber centered at $z = 0$, of length L, and $n_1=n(-L/2)$ and $n_2=n(L/2)$ then the equation (15) could be written as:

$$n(z) = \frac{\eta\dot{\Gamma}}{2A_c D}\left(\frac{L^2}{4} - z^2\right) + \frac{n_2 - n_1}{L} z + \frac{n_1 + n_2}{2}, \tag{16}$$

This parabolic solution is reached in an equilibrium state and depends only on η, the same as in the case of a warm vacuum chamber.

4 Photon flux along the long straight section

Due to the symmetry in IR1 and IR5 the SR entering the LSS in ring 1 lhs from the arc is identical to that entering the LSS in ring 2 rhs. Similarly the SR generated in D2 entering the LSS in ring 2 lhs is identical to that entering the LSS in ring 1 rhs. In this section the attenuation of SR from these sources is described with estimations on the effect of photon reflectivity. Finally the generation of SR from the quadrupole magnets, Q7, Q6, Q5, and Q4 within the LSS is considered.

4.1 Distance factor

The photon flux per meter in the LSS for the Ring 1, $\dot{\Gamma}_{LSS1}$, depends on the photon flux per meter in the arc, $\dot{\Gamma}_{arc} = 10^{17}$ photons/(s·m), and the distance, z, from the last bending magnet, MB, and can be expressed as:

$$\dot{\Gamma}_{LSS1}(z) = \dot{\Gamma}_{arc}\left(1 - \frac{z}{\sqrt{z^2 + R_{MB}d}}\right), \tag{17}$$

where R_{MB} is the MB bending radius and d is the diameter of the vacuum chamber. Direct photons, *i.e.* those not having undergone reflection, irradiate the straight region of the LSS from Q7 up to 1.9 m into the D2. In D2 the beam in ring 1, lhs, and ring 2, rhs, are steered towards the IP hence for geometrical reasons all direct photons from the arc cannot irradiate beyond 1.9 m inside D2.

The photon incident angle along the straight region is given by:

$$\theta_{LSS1}(z) = \frac{\sqrt{z^2 + R_{MB}d} - z}{R_{MB}}, \tag{18}$$

and ranges between 4.2 mrad close to the arc and 0.25 mrad close to D2, *i.e.* extremely grazing incidence.

In the vacuum chamber of D2 the photon incident angle is given by:

$$\theta_{D2}(z) = \theta_{LSS1}(z) + \frac{z - l_s}{R_{D2}}, \tag{19}$$

where R_{D2} is the D2 radius, l_s the distance between MB and D2.

In the same way, the photon flux per meter in LSS for the ring 2, $\dot{\Gamma}_{LSS}$, depends on the photon flux from D2, $\dot{\Gamma}_{D2} = 3 \cdot 10^{16}$ photons/(s·m), and the distance from D2, and can be expressed as:

$$\dot{\Gamma}_{LSS2}(x) = \dot{\Gamma}_{D2}\left(1 - \frac{x}{\sqrt{x^2 + R_{D2}d}}\right), \tag{20}$$

where R_{D2} is the D2 bending radius and $x = z - l_s$ is the distance from the end of D2 to the point irradiated. Direct photons from D2 irradiate the straight region of the LSS ring 2 lhs starting from about 18 m from the beginning of D2 (end of the cryostat) to the arc.

The photon incident angle along the straight region in ring 2 is given by:

$$\theta_{LSS2}(x) = \frac{\sqrt{x^2 + R_{D2}d} - x}{R_{D2}}, \tag{21}$$

SR from the dipole D1 irradiates part of the straight region, however, its photon flux on the vacuum chamber from D1 is about 5 times less than that from D2, and its critical energy is also a factor of 2.5 times smaller. Its influence on our estimations of gas density is therefore regarded as negligible.

4.2 Reflectivity factor

There exist two independent studies for the photon reflectivity on SR beam lines: on EPA at CERN [4] and on VEPP-2M at BINP [5]. Both demonstrate that for an average grazing incidence angle of 11 and 20 mrad respectively the forward scattered photon reflectivity may range from 2% for a ribbed Cu surface up to 95% for a 'smooth' co-laminated Cu.

Taking into account the forward scattered reflectivity factor, R, the photon flux per meter along the straight region of LSS and 1.9 m into the D2 dipole in can be given by:

$$\dot{\Gamma}_r(z) = \left[\dot{\Gamma}_s(z) + \sum_{n=1}^{n_{max}} \dot{\Gamma}_s\left(\frac{z}{2n+1}\right) \cdot R^n \cdot \frac{\theta(z)}{\theta\left(\frac{z}{2n+1}\right)} \right] \cdot (1-R), \tag{22}$$

and beyond 1.9 m in the D2 dipole as:

$$\dot{\Gamma}_r(z) = \left[\sum_{n=1}^{n_{max}} \dot{\Gamma}_s\left(\frac{z}{2n+1}\right) \cdot R^n \cdot \frac{\theta(z)}{\theta\left(\frac{z}{2n+1}\right)} \right] \cdot (1-R), \tag{23}$$

where n is the number of reflections to reach point z from point $z/(2n+1)$.

Figure 2 shows the photon flux in the LSS from the arc as a function of photon reflectivity of the vacuum chamber walls. It should be noted that it does not indicate the absorbed photon flux. The curve for R=0 is essentially identical to that shown for R=0.02 except that beyond 105 m the photon flux will be zero. The dilution of SR generated in D2 towards the arc is identical to that shown in Figure 2, from 0 m up to 105 m.

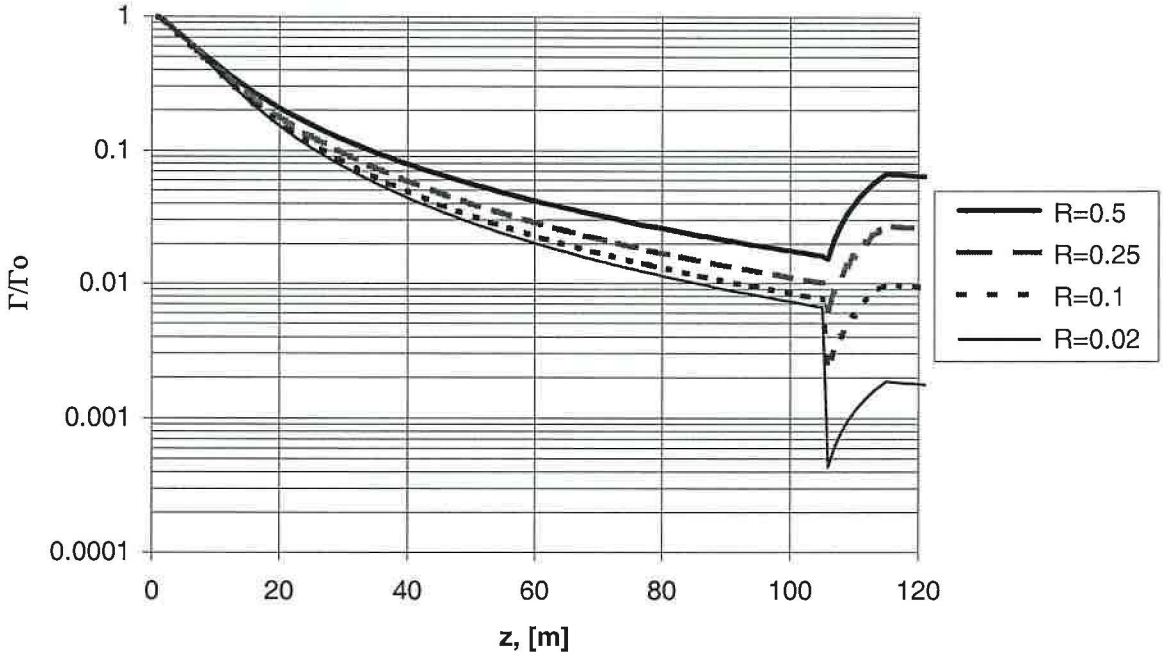

Figure 2. Photon flux from the arc along the LSS as a function of reflectivity.

4.3. SR from the quadrupoles

Calculations have been made to estimate the photon flux and critical energy for Q7, Q6, Q5, and Q4 based on the study of E. Keil [6].

For the beam size σ_{rms} = 0.3 mm and a closed-orbit of Δ = 4 mm and alignment tolerances of 1 mm the estimations are made with a magnetic field strength of 200 T/m for Q7 and 160 T/m for Q4, Q5 and Q6. In addition the beam orbit will be moved about 4 mm from the center of vacuum chamber in the collision regime, *i.e.* an offset of the beam Δ • 9 mm could reached in Q4.

There is no SR from a quadrupole when the circulating beam lies on–axis. The maximal photon flux is obtained when the beam has its maximum offset. The calculated critical energies, maximum linear photon fluxes generated from each element in the matching section, assuming zero photon reflectivity are given in Table 2. In addition the last two columns indicate the region of the LSS that these direct photons may irradiate. The elements in bold correspond to the

elements that will be irradiated with the maximum photon flux, *i.e.* when the beam has its maximum off-set passing through the source element. A range of values for the critical energy is given depending on how the offset is derived (linearly or quadratically).

Table 2. Sources of the SR in ring 1 and ring 2 of IR1 and IR5 indicating critical energies, maximan linear photon fluxes and the region of the LSS that these direct photons may irradiate.

SR source	ε_c, [eV]	$\dot{\Gamma}$, [photons/(s·m)]	Irradiates in ring 1	Irradiates in ring 2
D2	14.4	$< 2 \cdot 10^{16}$	TAN to D1	**Q4** to Arc
Q4	2–11	$< 2 \cdot 10^{15}$	**D2** to D1	**Q6** to Arc
Q5	0.5–7.5	$< 1.5 \cdot 10^{15}$	**D2** to D1	**Q7** to Arc
Q6	0.5–7.5	$< 1.5 \cdot 10^{15}$	**Q4 and D2** to D1	**Arc**
Q7	0.5–8.5	$< 3 \cdot 10^{15}$	**Q5** to D1	**Arc**
Arc	44.1	• $1 \cdot 10^{17}$	**Q7** to D1 See Figure 2	**Arc**

As an example let us consider the SR from Q7. If the beam in ring 1 lhs has a maximum offset in Q7 (4 mm closed orbit + 1 mm alignment tolerance) then the generated SR will have a critical energy of 8.5 eV. It will irradiate, with a maximum linear photon flux of $3 \cdot 10^{15}$ photons/(s·m), between 45 and 83 m downstream from the start of Q7, *i.e.* Q5 and adjacent regions. The linear photon flux in Q5 from the arc, see Figure 2 and Table 3, is comparable for the same low reflectivity. Since the critical energy is a factor of 5 smaller from Q7 than that from the arc, the photon induced gas density will be reduced by approximately the same factor. It can therefore be concluded that for a low photon reflectivity the SR from Q7 in ring 1 lhs is, even in exceptional conditions, insignificant in determining the gas densities.

Table 3. A comparison of the maximum linear photon fluxes from the quadupoles Q4-Q7 with that from the arc and D2 for ring 1 and ring 2, respectively, for low photon reflectivity.

	Ring 1 lhs		Ring 2 lhs	
Irradiated Element	Max. linear photon flux from Q7-Q4 [photons/(s·m)]	Linear photon flux from Arc [photons/(s·m)]	Max linear photon flux from Q4-Q7 [photons/(s·m)]	Linear photon flux from D2 [photons/(s·m)]
D2	$5 \cdot 10^{15}$	$7 \cdot 10^{14}$	0	0
Q4	$1.5 \cdot 10^{15}$	$8 \cdot 10^{14}$	0	0
Q5	$3 \cdot 10^{15}$	$1.5 \cdot 10^{15}$	0	$1 \cdot 10^{16}$
Q6	0	$6 \cdot 10^{15}$	$2 \cdot 10^{15}$	$3 \cdot 10^{15}$
Q7	0	$1 \cdot 10^{17}$	$1.5 \cdot 10^{15}$	$1.5 \cdot 10^{15}$
Arc	0	$1 \cdot 10^{17}$	$4.5 \cdot 10^{15}$	$1.5 \cdot 10^{15}$

In the case of Q6, for a low photon reflectivity, the SR generated will have a critical energy of 7.5eV with a linear photon flux of $< 1.5 \cdot 10^{15}$ photons/(s·m) between 44 and 81 m downstream from the start of Q6, *i.e.* upstream of Q4, Q4 and D2. Similarly to the Q7 case, it can be concluded that for low a photon reflectivity the SR from Q6 in ring 1 lhs is insignificant in determining the gas densities in Q4, however, on the other hand is comparable or even determines the gas density in D2. For a high photon reflectivity the SR from the arc will determine the gas density in D2. Similar arguments apply to the SR from Q5.

The situation in ring 2 lhs is somewhat clearer. From Table 3 it can be seen that the maximum linear photon fluxes generated by the quadrupoles are comparable to that from D2. Since the critical energy of SR from D2 is a factor of two larger than those from the quadrupoles the gas densities will be dominated by SR from D2.

In summary, for a high photon reflectivity (R=0.5), the gas densities in the LSS of IR1 and IR5 are dominated by the SR from the arc or D2 and the SR from the quadrupoles, Q7, Q6, Q5 and Q4 can be neglected. This is also true for a low photon reflectivity, except in D2 ring 1 lhs where the gas densities will be dominated by SR from Q4, Q5 and Q6. In the following determinations of the gas density it is therefore assumed, for simplicity, that the only sources of SR are from the arc dipole or D2.

5 Results of calculations

5.1 Input data

The experimental data to be used for estimation of the gas density inside the LHC vacuum chamber are given in a separate Note [7]. In that Note it was shown that the main gases in residual spectrum are H_2 and CO.

The general parameters and assumptions used in the estimations are given below:

- The diameter of tube or beam screen d=5.0 cm.
- R_{MB}=2784 m; R_{D1}=21543 m; R_{D2}=8518 m.
- The photon critical energy is ε_c=44.1 eV for SR from MB, ε_c=5.7 eV for D1 and ε_c=14.4 eV for D2.
- The mean molecular speed of photodesorbed molecules is $v=3.2\cdot10^4$ cm/s for H_2 and $v=8.4\cdot10^3$ cm/s for CO.
- The distributed pumping speed of the holes, $C = k_t \rho S$, where $k_t = 0.044$ is the ratio of the pumping holes area to whole vacuum chamber wall area, $\rho = 0.67$ is the Clausing factor and S is the ideal pumping speed.
- The desorption yields are independent of the photon incidence angle.
- The photon reflectivity is independent of photon energy and incidence angle.

For H_2 the following input data are assumed:

- The primary photodesorption yield in the arcs is $\eta=10^{-3}$ molecules/photon.
- The secondary photodesorption yield is not higher than η'=1 molecules/photon (at a surface coverage more than 1 monolayer) and could only be obtained for temperatures less than 4.5 K.
- The sticking probability α was varied from 1 (corresponding T = 1.9 K), 0.1 (corresponding T=4.5 K) down to 10^{-5} (for temperatures higher than 4.5K).

For CO the following input data are assumed:

- The primary photodesorption yield in the arcs is η=10^{-4} molecules/photon.
- CO_2 is cracked to form CO and O_2 and the amount of condensed CO is a sum of desorbed CO and CO_2 molecules. It is assumed that the surface density of condensed CO and CO_2 will not exceed a few tenths of monolayer and CH_4 will not exceed one monolayer. In which case the secondary photodesorption yield is assumed be less than η'= ~ 10^{-3} molecules/photon corresponding to $5 \cdot 10^{16}$ molecules/cm^2; saturation occurs at η'= 0.04 molecules/photon (at surface coverage more then 10^{19} molecules/cm^2)[8].
- The sticking probability α was varied from 1 down to 0.001.

5.2. Results

Figures 3 and 4 show the estimated axial H_2 and CO density distribution $n(z,\sigma,\eta,\eta')$ for the v6.0 in the LSS of IR1 and IR5 from the arc to D2 with beam screens and operating temperatures given in Table 1. There it is assumed that SR from the quadrupoles is negligible and the only source of SR is either MB or D2, as discussed in section 4.3. Unless stated the photon reflectivity is assumed to be 0.02. These figures therefore indicate the minimum gas densities in these LSS; maximum values could be a factor of five higher in specific locations such as D2 for low reflectivities. The results for the H_2 density distribution are shown for a photon reflectivity of 0.02 and 0.5. The estimated H_2 density distribution will be reached after about one or two days of LHC operation, whereas the estimated CO density will only be obtained after three years of LHC operation (assuming that the machine is not warmed up during this period). The initial CO density will be one order of magnitude lower than that indicated. The average gas densities of H_2 and CO are $1.7 \cdot 10^9$ and $5 \cdot 10^6$ molecules/cm^3 respectively.

Figures 5 and 6 show the axial H_2 gas density distribution $n(z,\alpha,\eta,\eta')$ for various operating conditions, namely 4.5 K and 1.9 K, with and without beam screens. There are three different curves shown:

1. All the vacuum chambers are held at T=4.5 K. The quadrupoles Q4–Q7 are without a beam screen whilst all others contain a beam screen;
2. All the vacuum chambers are held at T=1.9 K. The quadrupoles Q4–Q7 are without a beam screen whilst all others contain a beam screen;

3. All the vacuum chambers are held at T=1.9 K and contain a beam screen;

These curves serve to describe all feasible combinations of temperature and presence of a beam screen. A curve for the vacuum chambers at T = 4.5 K without a beam screen is not shown since a H_2 coverage of one monolayer (accumulated after approximately ten days of LHC operation) will result in the gas density to rise to its equilibrium gas density, *i.e.* to an unacceptable level.

A vacuum chamber with a beam screen requires that the surrounding cold bore be at either at 1.9 K or at 4.5 K with a cryosorber thereby providing a sufficiently high pumping capacity, otherwise the equilibrium H_2 density will be reached after a few days of LHC operation.

Figures 3 and 5 correspond to ring 1 lhs in which the LSS vacuum chamber walls are irradiated by SR from MB. Figures 4 and 6 correspond to Ring 2 lhs in which the LSS vacuum chamber walls are irradiated by SR from D2.

The axial gas density distribution $n(z)$ for H_2 at $\eta = 10^{-4}$ molecules/photon results in similar plots except with an order of magnitude lower density.

The gas density in ring 1 for CO is highest in the arc and in Q7. For α=1, the gas density, with or without a beam screen, will equal $3 \cdot 10^7$ molecules/cm^3. However for α<1, the gas density without a beam screen will be inversely proportional to α. For example would correspond to $3 \cdot 10^8$ molecules/cm^3 for α=0.1. For a vacuum chamber with a beam screen the gas density will be limited by the pumping speed of the pumping holes. It will range between $9 \cdot 10^8$ molecules/cm^3 for α<0.001 with most of the gas being pumped through the holes, to $3 \cdot 10^7$ molecules/cm^3 for α=1 with most of gas remaining on the beam screen.

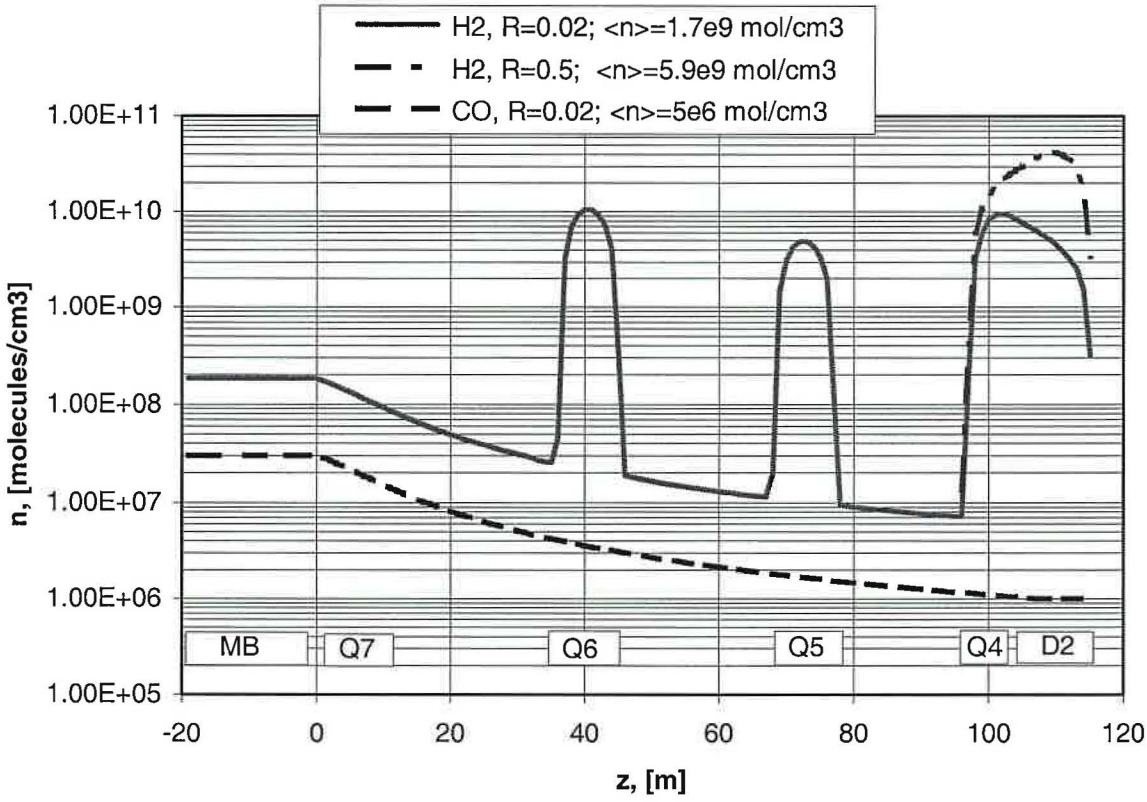

Figure 3. The axial gas density distribution n(z) for H_2 and CO in IR1 and IR5 for ring 1 lhs for optics v6.0. The sticking probability of CO is assumed to be unity.

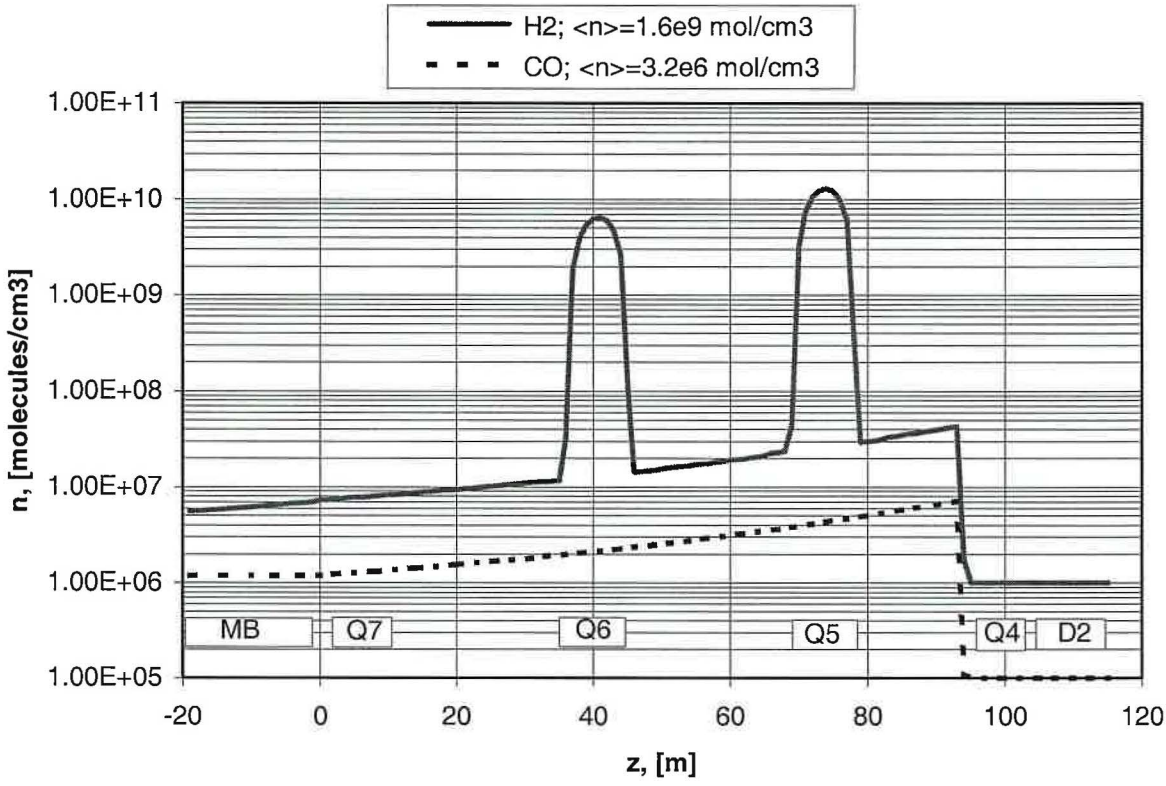

Figure 4. The axial gas density distribution n(z) for H_2 and CO in IR1 and IR5 for ring 2 lhs for optics v6.0. The sticking probability of CO is assumed to be unity.

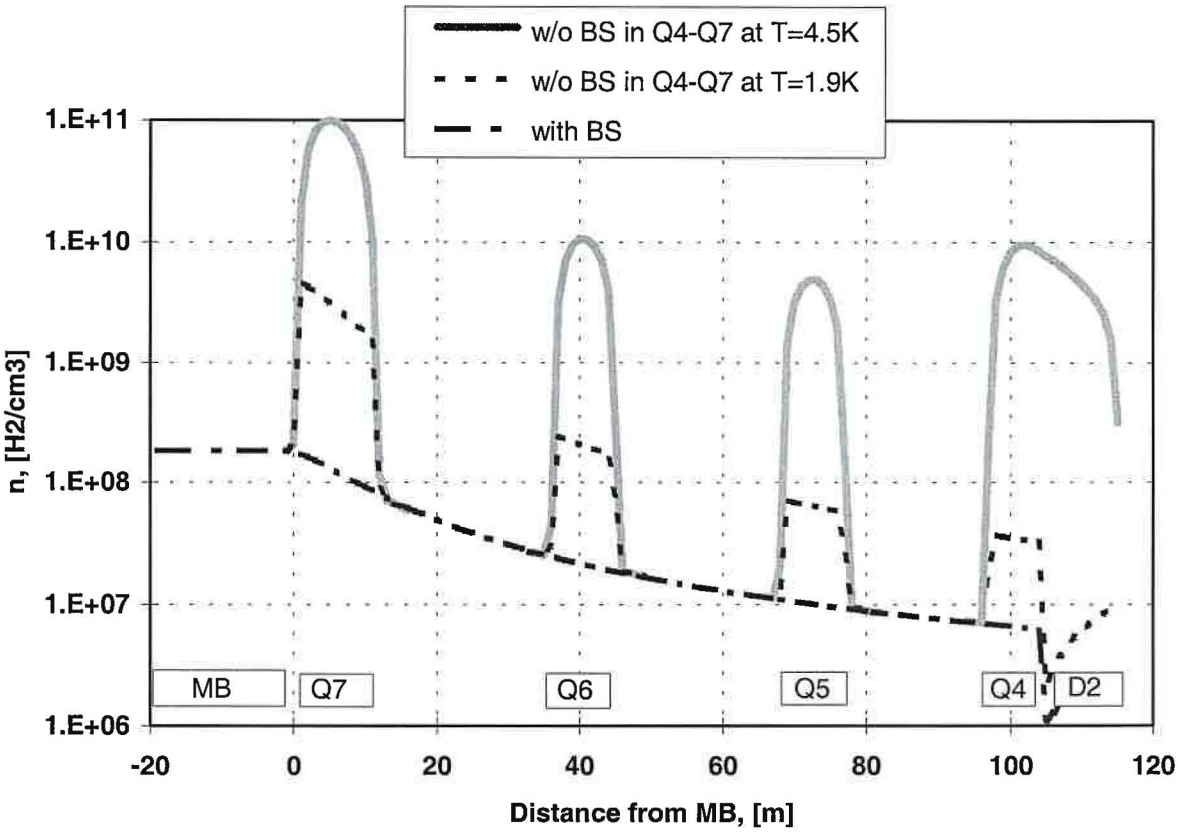

Figure 5. The axial gas density distribution n(z) for H_2 in IR1 and IR5 for the ring 1 lhs.

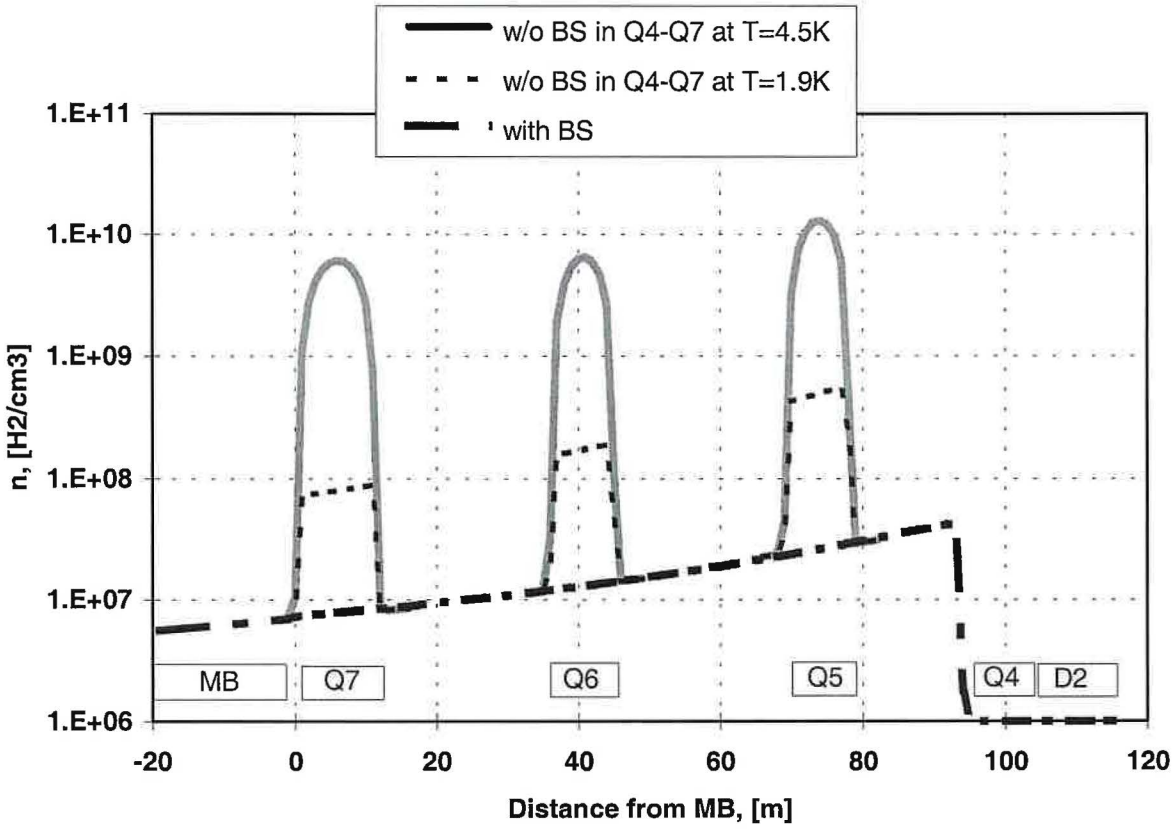

Figure 6. The axial gas density distribution n(z) for H_2 in IR1 and IR5 for ring 2 lhs.

6. Discussion

For LHC optics v6.0 the average gas density, due to photodesorption, in ring 1 lhs for H_2 and CO are $1.7 \cdot 10^9$ and $5 \cdot 10^6$ molecules/cm^3 respectively for a low photon reflectivity (R=0.02) and $5.8 \cdot 10^9$ molecules/cm^3 for H_2 for a high photon reflectivity (R=0.5). In order to limit the background in the LHC experiments from beam-gas interactions generated upstream of the experiments a rate of $< 4 \cdot 10^6$ events/s [9] has been defined. This rate therefore puts an upper limit on the average gas density in the LSS ring 1 lhs and ring 2 rhs, corresponding to an average H_2 density of $5 \cdot 10^8$ molecules/cm^3 over the 268.9m LSS [10]. If one assumes that H_2 is the only gas in the system and the estimated average density is representative over the LSS then the beam-gas interaction background in the experiments would be approximately $1.4 \cdot 10^7$ events/s and $4.6 \cdot 10^7$ events/s for a low and high photon reflectivity, respectively. Moreover, the gas density is not only composed of H_2 molecules but also contains CH_4, CO, and CO_2 with larger proton gas scattering cross-sections, by a factor of 6, 9 and 14 respectively [11], thereby increasing this estimated background rate. One might argue that during commissioning of the machine that the initial desorption yield will be reduced by a factor of say ten and therefore the background due to beam-gas interaction will be reduced by a corresponding factor. However, taking into account the approximations and uncertainties in the estimations of the gas densities due to photodesorption and in addition, noting that other mechanisms such as electron and ion bombardment will add to these estimated gas densities it is therefore prudent to minimise the gas densities wherever feasible. An obvious solution would be to incorporate a beam screen (with or without active cooling) into each cryogenic element of the LSS. In doing so the average H_2 density, due to photodesorption, in ring 1 lhs would be reduced by a factor of over 50 to $3.2 \cdot 10^7$ molecules/cm^3 for a reflectivity of 0.02. In addition such a solution would exclude any potential vacuum instability due to ion induced desorption, to be addressed in a future note.

7. Conclusions

Estimations of the SR critical energies and photon fluxes from the arc, D2, D1 and quadrupoles for optics v6.0 in the LSS of IR1 and IR5 are presented. For a high photon reflectivity (R=0.5) the SR from arc dominates over the quadrupoles Q4, Q5, Q6 and Q7 in the estimation of the gas densities in the LSS of IR1 and IR5. This is also true for a low photon reflectivity (R=0.02), except for D2 in ring 1 lhs where the SR from Q4, Q5 and Q6 will dominate. The average gas density, due to photodesorption assuming SR from the arc only, in ring 1 lhs for H_2 and CO are $1.7 \cdot 10^9$ and $5 \cdot 10^6$ molecules/cm^3 respectively for a low reflectivity and $5.8 \cdot 10^9$ molecules/cm^3 for H_2 for a high photon reflectivity. The average gas densities, due to photodesorption assuming SR from D2 only, in ring 2 lhs for H_2 and CO are 1.6 10^9 and $3.2 \cdot 10^6$ molecules/cm^3 respectively for a low photon reflectivity.

These estimations are comparable to the upper limit of the gas density set by the background rate of $4 \cdot 10^6$ events/s in the LHC experiments generated upstream by the proton-gas interactions. A solution to reduce the average gas density in the LSS would be to install a beam screen (with or without active cooling) into the cryogenic elements. Such a solution would also exclude any potential vacuum instability caused by ion induced desorption.

The estimations of the gas densities presented here are made for LHC optics version 6.0. The layout of Q7 to D2 has changed slightly in going to optics version 6.1. A section of warm vacuum chamber has been introduced in between Q4 and Q5 for the possible installation of Roman pots and Q6 and Q5 will operate at 1.9 K; all other parameters remain unchanged. Since the photon fluxes estimated here are unchanged the main conclusions should also be valid for optics version 6.1. The gas density profiles for v6.1 can be extracted from Figure 5 and 6.

References:

[1] E. Wallén, "Synchrotron radiation in the interaction regions of the LHC", CERN/ AT-DI/92-30, LHC Note 210.

[2] V.V. Anashin, O.B. Malyshev, V.N. Osipov, I.L. Maslennikov and W.C. Turner. "Investigation of synchrotron radiation-induced photodesorption in cryosorbing quasi-closed geometry", J.Vac.Sci.Technol. A 12(5), pp. 2917–2921, Sep/Oct 1994.

[3] W. Turner. "Beam tube vacuum in future superconducting proton colliders", SSCL-Preprint-564, Oct 1994.

[4] V. Baglin, I.R. Collins and O. Gröbner. "Photoelectron yield and photon reflectivity from candidate LHC vacuum chamber materials with implications to the vacuum chamber design" LHC Project Report 206.

[5] V.V. Anashin, O.B. Malyshev, N.V. Fedorov, V.P. Nazmov, B.G. Goldenberg, I.R. Collins and O. Gröbner, "Reflection of photons and azimuthal distribution of photoelectrons in a cylindrical beam pipe", LHC Project Report 266.

[6] E. Keil. "Synchrotron radiation from a large electron-positron storage ring", CERN/ISR-LTD/76-23

[7] O.B. Malyshev, V.V. Anashin, I.R. Collins and O. Gröbner. "Photodesorption processes including cracking of molecules in a cryogenic vacuum chamber" Vacuum Technical Note in preparation, September 1999.

[8] V.V. Anashin, O.B. Malyshev, R. Calder and O. Gröbner, "A study of the photodesorption process for cryosorbed layers of H_2, CH_4, CO or CO_2 at various temperatures between 3K and 68K". Vacuum **53**, 269-272 (1999)

[9] J-B. Jeanneret, "Workshop on LHC backgrounds", 22 March 1996

[10] J-B. Jeanneret, private communication 3/9/99

[11] K.Eggert, K. Honkavaara and A. Morsch, LHC Note 263, 8th February, 1994